ACS NANO MEDICINE

pubs.acs.org/ACSNanoMed Article

Programmable Modular Peptide Nanocarriers for Targeted siRNA Delivery to Immune Cells

Nan Kong, Yueying Liu, Liheng Lu, and Huaimin Wang*

Cite This: https://doi.org/10.1021/acsnanomed.5c00151 Read Online

ACCESS | Metrics & More | Article Recommendations | Supporting Information

ABSTRACT: Genetically engineered immune cell therapies have achieved significant progress in treating various diseases. However, efficiently and selectively delivering genetic material to specific immune cells remains a major challenge. In this study, we developed a modular peptide-based system for the targeted delivery of siRNA to immune cells, including macrophages, dendritic cells, and T cells. The system consists of three functional modules: a hydrophilic cell-penetrating peptide module for efficient membrane penetration, an RNA-binding sequence for siRNA encapsulation, and immune cell-targeting motifs for specific recognition. The results show that the rationally designed peptide system achieves 80−90% siRNA delivery efficiency in macrophages and dendritic cells in vitro compared to 15% in T cells when using the unmodified peptide. By modifying the peptide with cell-specific targeting motifs, we enhanced siRNA delivery efficiency in T cells to ∼60%. Furthermore, in a tumor model, our system selectively delivers siRNA to target immune cells, with CRM achieving 41% siRNA delivery to macrophages, significantly higher than that of the baseline peptide. This modular peptide-based approach provides a robust and scalable platform for efficient gene delivery to immune cells, offering the potential for advancing therapeutic applications in immune modulation and related diseases.

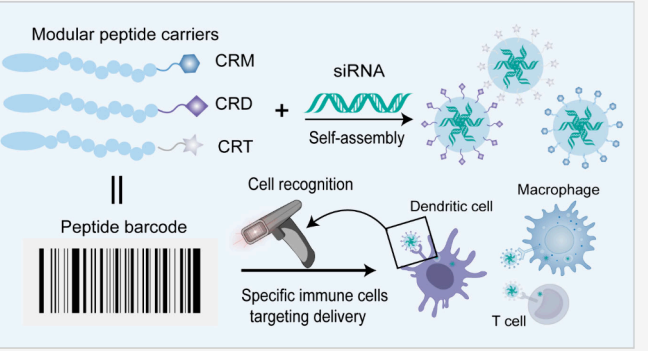

KEYWORDS: *peptide, gene delivery, self-assembly, tumor microenvironment, targeting immune cells, nanoparticle*

INTRODUCTION

Gene-engineered immune cell therapies have achieved notable clinical progress and hold promising therapeutic potential for treating diseases, such as cancer, fibrosis, and infections.[1−4] For example, targeted delivery of mRNA encoding chimeric antigen receptors (CAR) or interferon regulatory factor 5 (IRF5) to macrophages within the tumor microenvironment (TME) represents a promising approach for cancer therapy.[5−7] In addition, macrophage-targeted siRNA delivery to silence TGF-β1 was employed in the treatment of lung fibrosis.[8] Dendritic cells (DCs) are pivotal in antigen presentation and the initiation of antigen-specific immune responses, highlighting their critical role in vaccine development.[9] Clinical trials have demonstrated that dendritic cell mRNA vaccines are safe and effective for treating respiratory syncytial virus (RSV) infection (NCT05127434), pancreatic cancer (NCT04157127), and neuroblastoma (NCT04837547).[10] Furthermore, in autoimmune disorders, targeted delivery of microRNA-125a to regulatory T cells (Tregs) significantly attenuated the progression of systemic lupus erythematosus (SLE).[11,12] In oncology, engineered T cells expressing chimeric antigen receptors have achieved remarkable success in treating hematological malignancies.[13] However, targeted gene delivery to T cells remains particularly challenging due to several intrinsic biological barriers. T cells are relatively scarce within the tumor microenvironment, exhibit low endocytic activity, and possess a high nucleus-to-cytoplasm ratio, all of which limit intracellular accumulation of nucleic acid cargos. In addition, T cells express low levels of heparan sulfate proteoglycans, which are commonly exploited by cationic delivery systems for cellular uptake.[14]

The major bottleneck in engineered immune cell therapy lies in the development of highly efficient, safe, and cell-specific delivery systems.[15] CAR-T cell therapies approved by the FDA are typically engineered ex vivo using lentiviral vectors.[16] In additional, adeno-associated viruses (AAV) have shown greater clinical progress in treating certain genetic diseases like inherited retinal dystrophy, but are limited by its packaging capacity.[17,18] To achieve targeted delivery, viral vectors are engineered with site-specific mutations in envelope glycoproteins, enabling selective binding to target cell surface

Received: November 15, 2025
Revised: February 5, 2026
Accepted: February 5, 2026

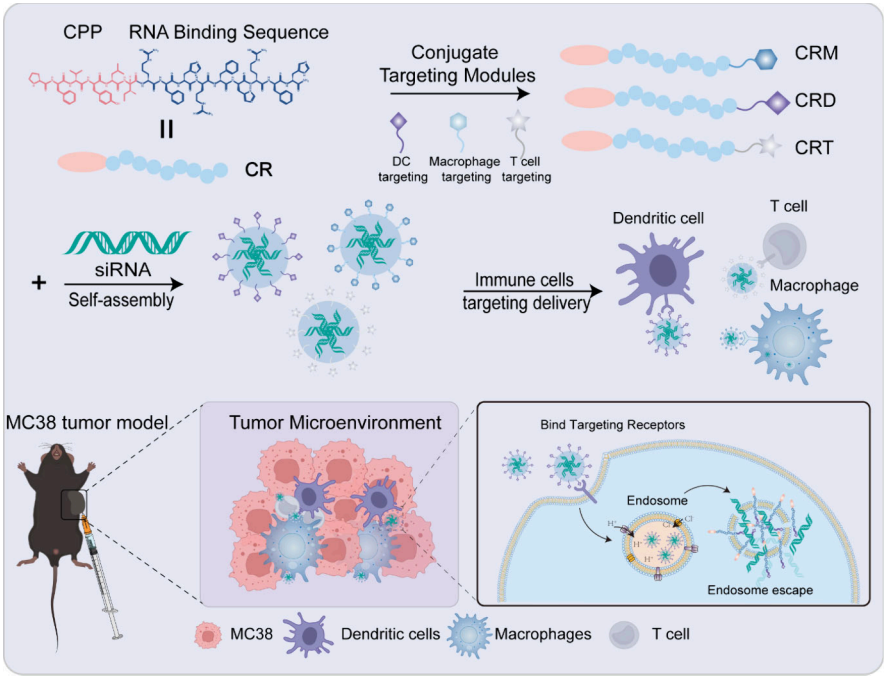

Figure 1. Schematic illustration of the programmable modular peptides designed for targeted siRNA delivery to immune cells in vitro and in the TME. **CRM**: Macrophages targeting delivery peptide. **CRD**: Dendritic cells targeting delivery peptide. **CRT**: T cells targeting the delivery peptide.

receptors.[19,20] However, such engineering is complex and does not entirely resolve issues of efficiency and safety in immune cell targeting.[21]

In addition, nonviral delivery systems, including polymers and LNPs, have made substantial advances in gene delivery to immune cells.[22] Among them, LNPs are the most widely used gene delivery systems in both clinical and research settings, due to their remarkable success in the COVID-19 vaccines.[23] However, selective transfection of immune cell subsets with high efficiency and specificity remains a challenge for LNP and polymers.[22,24] At present, the conjugation of targeting moieties, such as monoclonal antibodies or targeting peptides, is one of the most commonly used strategies to enhance immune cell-specific delivery of RNA therapeutics.[25−27] These approaches, while effective, often involve complex chemistries and may suffer from limited specificity or delivery efficiency in vivo.[28,29] Recent advances in nanocarrier systems, including antibody decorated lipid nanoparticles and mucoadhesive polymer coated particles, have extended the toolkit for targeted delivery by modulating surface properties and ligand−receptor interactions.[30,31] Peptide-mediated delivery represents a promising alternative, offering a low-cost, simple system in which peptides are simply mixed with gene cargos.[32−35] The use of peptide for gene delivery mainly refers to cell penetration peptide (CPP) including TAT, but the high cytotoxicity and insufficient targeting specificity hindered its application.[36,37]

Therefore, we sought to develop a modular peptide-based system for the targeted delivery of siRNA to specific immune cells. We first developed a general delivery platform composed of a hydrophobic cell-penetrating peptide (PFVYLI) and nucleic acid-binding unit repeat $(RFH)_3$, named as **CR** (Figure 1). To improve siRNA delivery efficiency and achieve cell-specific targeting, we incorporated a targeting module at the N-terminus of **CR** for targeting the delivery of siRNA to specific immune cells, macrophages, dendritic cells, and T cells. N-terminal mannose modification of the CR peptide improves macrophages selectivity by targeting mannose receptors on the macrophage membrane.[38] We incorporated the DC-targeting peptide sequence CLGPLGFTKVD, identified through phage display screening, to achieve dendritic cell (DC)-specific targeting.[39] To facilitate T cell targeting, we incorporated the established T cell-targeting peptide VVNPAEG into our peptide system, which enhances binding affinity to the mouse T cell surface receptor QA-2.[40] After modifying the T cell-targeted peptide sequence, the siRNA delivery efficiency was improved using peptide **CRT**, compared with **CR**. Furthermore, the modular peptide-based gene delivery systems enable precise delivery of siRNA to targeted immune cells in a coculture model and in more complex environments like the TME (Figure 1).

RESULTS AND DISCUSSION

Modular Peptide-Based Gene Delivery System

We first constructed a peptide-based gene delivery system composed of a cell-penetrating peptide and an RNA-binding sequence, designated as **CR** (Figure S1). We assessed the cytotoxicity of peptide **CR** in BMDMs, BMDCs, and CTLL-2 cells, respectively. No significant cytotoxicity was observed at a concentration of 100 μM (N/P = 20) across all tested immune cell types, suggesting the biocompatibility of the system (Figure 2A−C). To evaluate its effectiveness, we assessed the siRNA transduction efficiency of peptide **CR** in bone marrow-derived macrophages (BMDMs) following 6 h of transfection. Confocal laser scanning microscopy (CLSM) showed that peptide CR effectively delivers siRNA into BMDMs at N/P ratios of >12 (Figure 2D). At an N/P ratio of 12, the siRNA delivery efficiency reached approximately 80%, as quantified by flow cytometry (Figure 2E, Figure S2).

We then evaluated the ability of peptide **CR** to deliver siRNA to bone marrow-derived dendritic cells (BMDCs). CLSM imaging revealed that the mean fluorescence intensity

https://doi.org/10.1021/acsnanomed.5c00151
ACS Nano Med. XXXX, XXX, XXX−XXX

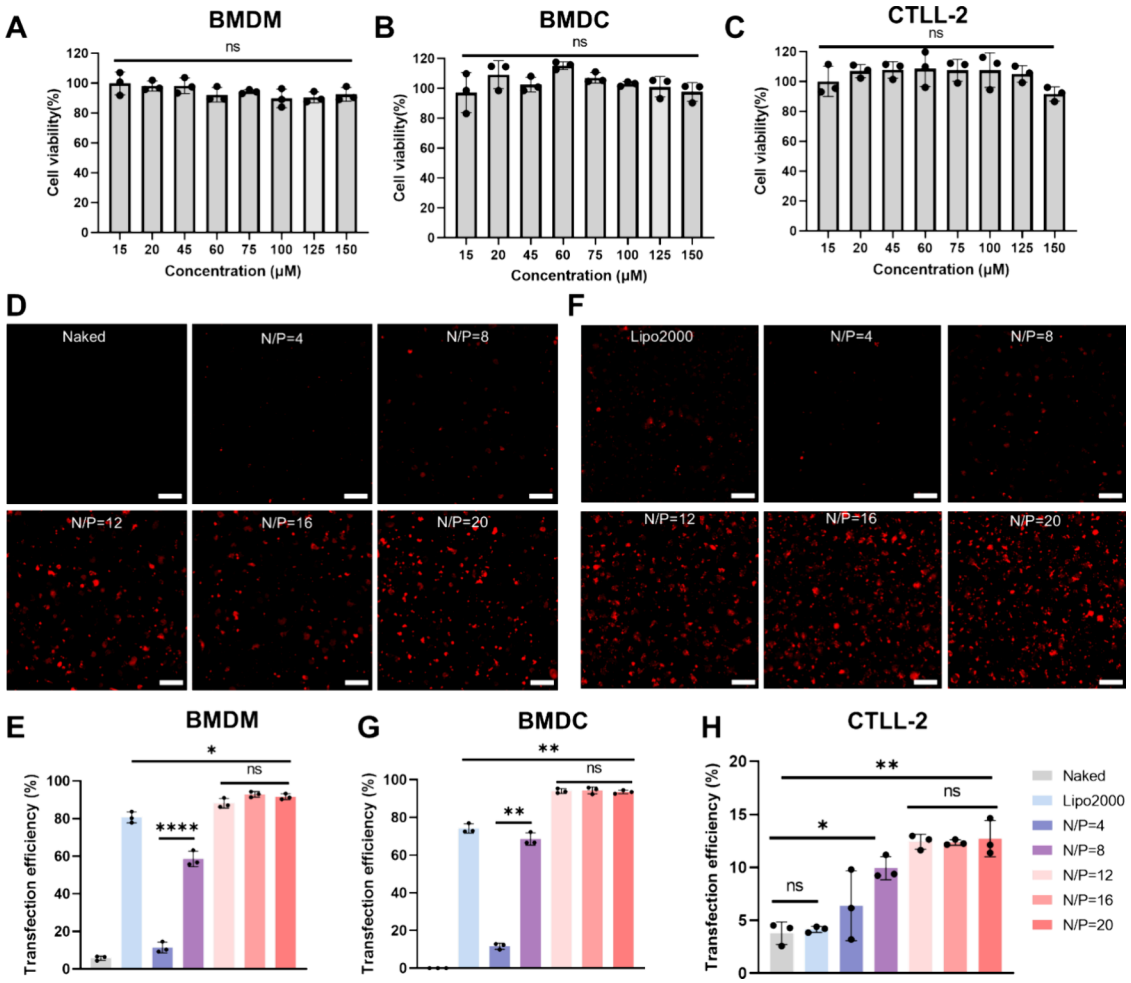

Figure 2. The cytotoxicity and siRNA transfection efficiency of peptide **CR** in different immune cells. (A–C) 24 h cytotoxicity of peptide **CR** against (A) BMDMs, (B) BMDCs, and (C) CTLL-2 cells, respectively. (D) Representative CLSM images of BMDM after transfected with siRNA-Cy5 using peptide CPP-RFH_3 (**CR**). Scale bar is 50 μm. (E) siRNA delivery efficiency of peptide **CR** in BMDMs after 6 h of treatment. (F) Representative CLSM images of BMDCs after transfected with siRNA-Cy5 using peptide CR. Scale bar is 50 μm. (G) siRNA delivery efficiency of peptide **CR** in BMDCs after 6 h of treatment. (H) siRNA delivery efficiency of peptide **CR** in CTLL-2 cells after 6 h of treatment. Data are depicted as mean ± SD. Statistical analysis is calculated using one-way ANOVA analysis: *p < 0.05, **p < 0.01, ***p < 0.001, and ****p < 0.0001.

(MFI) in the CR group at an N/P ratio of 12 was higher than that in the Lipo2000 group, 6 h post-transfection (Figure 2F, Figure S3). Flow cytometry analysis showed that peptide **CR** achieved an approximately 90% siRNA delivery efficiency in BMDCs (Figure 2G, Figure S4). Next, we tested the delivery efficiency of peptide **CR** in CTLL-2 cells. While peptide **CR** exhibited effective transfection in BMDMs and BMDCs, it showed only approximately 15% siRNA delivery efficiency in CTLL-2 cells (Figure 2H).

Targeted Delivery of siRNA to Macrophages with Modular Peptide CRM

To enhance targeted delivery of siRNA to macrophages and improve delivery efficiency both in vitro and in vivo, we modified peptide **CR** by conjugating it with mannose, resulting in a macrophage-targeting delivery system, designated as **CRM** (Figure S5). Notably, the CLSM results indicated that peptide **CRM** achieved effective siRNA delivery to BMDMs at an N/P ratio of 4 (Figure 3A). Furthermore, **CRM** exhibited a significantly higher siRNA delivery efficiency than CR at the same N/P ratio (Figure S6). Flow cytometry analysis revealed that siRNA delivery efficiency reached 80% at an N/P ratio of 4, with nearly complete delivery (approaching 100%) at N/P ratios of 8 (Figure 3B). Moreover, **CRM** exhibited superior biocompatibility relative to **CR**, demonstrating no cytotoxicity in BMDMs at a concentration of 200 μM (Figure 3C). These results suggest that **CRM** enhances the siRNA delivery efficiency while maintaining favorable safety profiles.

We next investigated the morphology of siRNA/CRM nanoparticles using cryo-electron microscopy (Cryo-EM), which revealed that peptide **CRM** and siRNA coassembled into well-defined nanospheres with an average diameter of 60 nm at an N/P ratio of 20 (Figure 3D). Hydrodynamic diameters of siRNA/CRM nanoparticles were further analyzed by using dynamic light scattering (DLS) across various N/P ratios. DLS measurements indicated that the average diameter of siRNA/CRM NPs was approximately 100 nm at an N/P ratio of 8, decreasing to about 60 nm at an N/P ratio of 20 (Figure 3E). The observed size reduction with an increasing N/P ratio may be attributed to the enhanced condensation of siRNA by peptide **CRM**, which could facilitate more efficient cellular uptake.

To explore the underlying cause of this size reduction, we examined the morphology of siRNA/CRM NPs at different N/P ratios by using transmission electron microscopy (TEM).

https://doi.org/10.1021/acsnanomed.5c00151
ACS Nano Med. XXXX, XXX, XXX−XXX

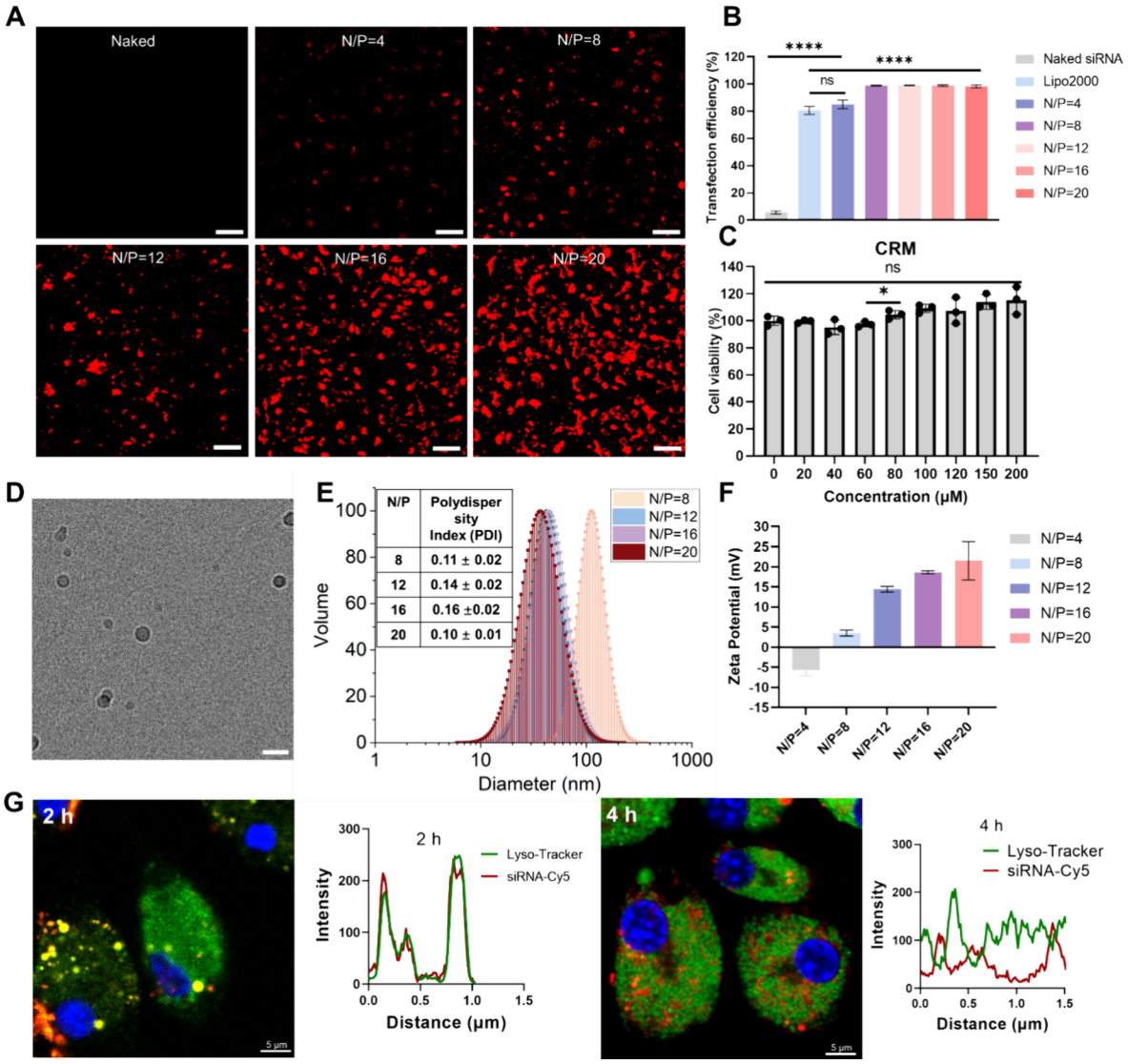

Figure 3. Macrophages-targeted siRNA delivery with peptide **CRM**. (A) Representative CLSM images of BMDMs transfected with siRNA-Cy5 using peptide **CRM**. Scale bar is 50 μm. (B) Quantification of siRNA delivery efficiency in BMDMs after treatment with peptide **CRM** for 6 h. (C) 24 h-cytotoxicity of peptide **CRM** against BMDMs. (D) Cryo-EM image of siRNA/CRM nanoparticles (N/P = 20). Scale bar is 100 nm. (E) DLS analysis of siRNA/CRM NPs at various N/P ratios. (F) Zeta potential of siRNA/**CRM** NPs at different N/P ratios. (G) Endosome escape of siRNA/**CRM** NPs in BMDMs. Lyso-Tracker shows green and siRNA-Cy5 is red. Scale bar is 5 μm. Data are depicted as mean ± SD. Statistical analysis is calculated using one-way ANOVA analysis. *p < 0.05, **p < 0.01, ***p < 0.001, and ****p < 0.0001.

TEM images revealed nanoaggregates at N/P ratios of 4, 8, and 12, while at N/P 20, the particles coassembled into well-defined nanoparticles (Figure S7). Cryo-EM further confirmed the nanoparticle morphology, showing consistent features under physiological conditions (Figure S8). Notably, the zeta potential of siRNA/CRM assemblies increased with rising N/P ratios, reaching approximately +20 mV at N/P ratio 20 (Figure 3F), suggesting that the increased surface charge contributes to nanoparticle stability and prevents aggregation.[41] Finally, confocal laser scanning microscopy (CLSM) analysis revealed that siRNA/CRM NPs colocalized with lysosomes at 2 h, with a Pearson's correlation coefficient of 0.85. After 4 h of incubation, the siRNA/CRM NPs had largely escaped the lysosomal compartments (Figure 3G), indicating successful endosomal escape, a critical step for efficient siRNA delivery. At low pH in lysosome, the peptide CRM disrupted membrane, facilitating siRNA endosome escape.[42]

Dendritic Cells Targeted siRNA Delivery with Peptide CRD

To enable targeted delivery of siRNA to dendritic cells, we conjugated CR with a CD11c-specific targeting peptide sequence CLGPLGFTKVD identified through phage display,[39] designated as **CRD** (Figure S9). **CRD** effectively delivered siRNA to DCs across various N/P ratios (Figure S10 and S11). However, **CRD** exhibited cytotoxicity toward BMDCs, reducing cell viability to 70% at a concentration of 100 μM (N/P = 20) and further decreasing cell viability to 45% at 200 μM (Figure S12). To mitigate this toxicity, we optimized the N/P ratio and found that **CRD** achieved approximately 90% siRNA delivery efficiency in BMDCs at an N/P ratio of 4, indicating a high transfection efficiency under milder conditions (Figure 4A, B). Furthermore, siRNA/CRD complexes did not exhibit obvious cytotoxicity to DC at N/P ratios ranging from 1 to 4 (Figure 4C).

Next, we characterized the siRNA/CRD complexes using TEM, which revealed that peptide **CRD** and siRNA

https://doi.org/10.1021/acsnanomed.5c00151
ACS Nano Med. XXXX, XXX, XXX−XXX

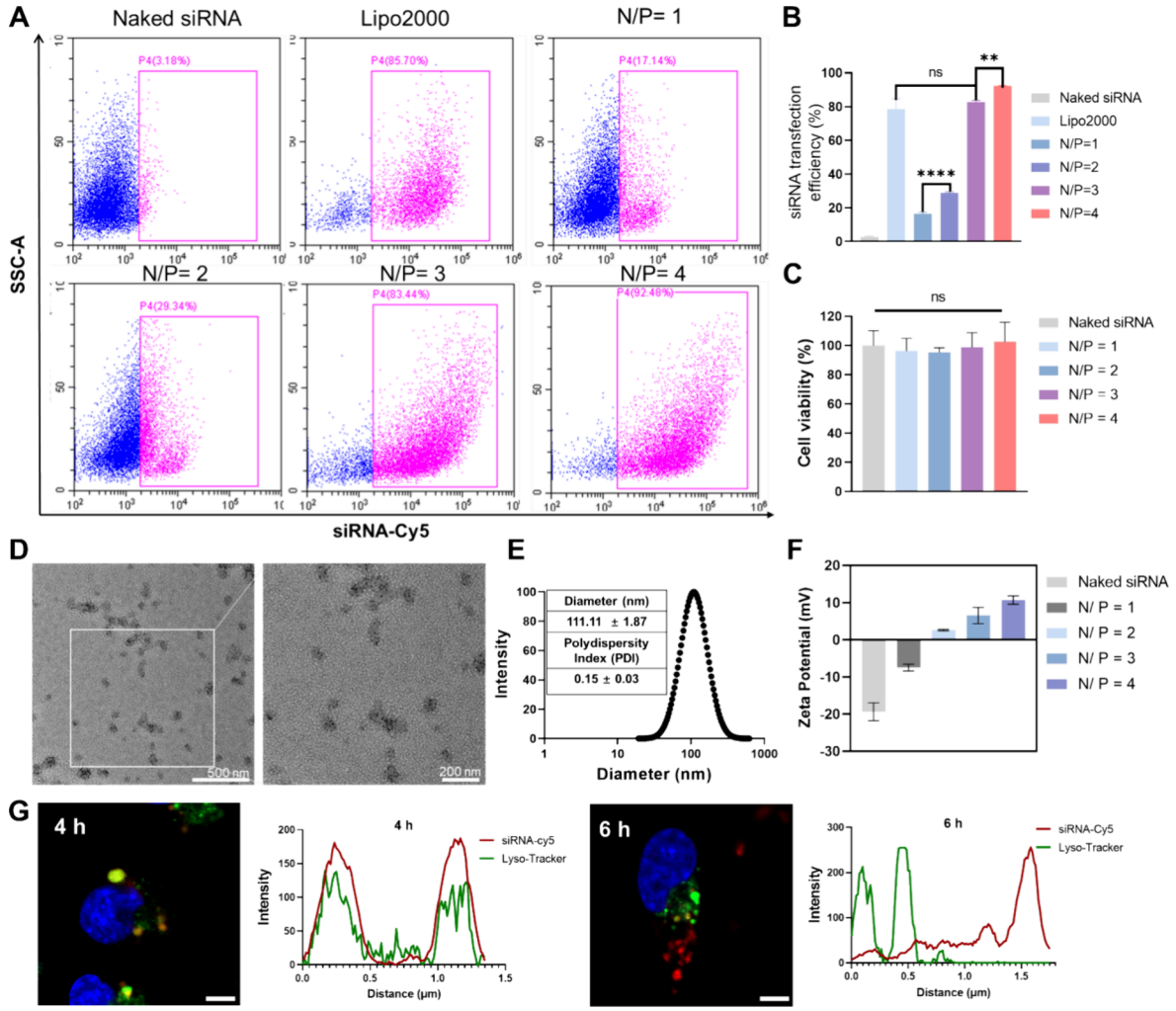

Figure 4. DC-targeted siRNA delivery with the peptide **CRD**. (A) Flow cytometry analysis of BMDCs after transfected siRNA-Cy5 using peptide **CRD** for 6 h. (B) Quantification of siRNA delivery efficiency in BMDCs after treatment with peptide **CRD** for 6 h. (C) Cytotoxicity of peptide siRNA/CRD NPs against BMDCs after treatment for 24 h at various N/P ratios. (D) TEM images of siRNA/**CRD** NPs at an N/P ratio of 4. (E) DLS analysis of siRNA/**CRD** NPs at an N/P ratio of 4. (F) Zeta potential of siRNA/**CRD** NPs at different N/P ratios. (G) Endosome escape of siRNA/**CRD** NPs in DC2.4, Lyso-Tracker shows green and siRNA-Cy5 is red. Scale bar is 5 μm. Data are depicted as mean ± SD. Statistical analysis is calculated using one-way ANOVA analysis. *p < 0.05, **p < 0.01, ***p < 0.001, and ****p < 0.0001.

coassembled into nanoparticles (Figure 4D). Dynamic light scattering (DLS) results showed that **CRD** and siRNA self-assembled into nanoparticles with a hydrodynamic diameter of approximately 100 nm at an N/P ratio of 4 (Figure 4E, Figure S13). Zeta potential measurements of siRNA/CRD complexes across various N/P ratios showed a progressive increase in surface charge with increasing N/P values, reaching approximately +10 mV at an N/P ratio of 4 (Figure 4F).

Endosomal escape represents a major challenge for most gene delivery systems seeking to achieve efficient intracellular delivery in DCs, primarily due to the abundant lysosomes in these innate immune cells.[43] To further investigate the cellular uptake and endosomal escape of siRNA/CRD nanoparticles (NPs), we performed CLSM analysis of DC2.4 cells transfected with siRNA-Cy5 with the **CRD** peptide at various time points. At 2h post-transfection, a portion of the siRNA/CRD NPs had been internalized, while some remained binding with the cell membrane (Figure S14). CLSM analysis revealed significant colocalization of siRNA/CRD nanoparticles with lysosomes at 4 h post-transfection, suggesting that the internalized complexes follow endolysosomal trafficking routes.[44,45] By 6 h, however, the siRNA/CRD NPs had largely escaped the endosomal compartments, thereby avoiding lysosomal degradation (Figure 4G).

T cells Targeted siRNA Delivery with Peptide CRT

We optimized the modular peptide-based targeting siRNA delivery system by conjugating a T cell- targeted peptide sequence, VVNPAEG, to improve both delivery efficiency and specific targeting of siRNA to T cells (Figure S15).[40] We next characterized the morphology of siRNA/CRT assemblies using transmission electron microscopy (TEM), which revealed that peptide **CRT** and siRNA coassembled into nanospheres with an average diameter of 50 nm at an N/P ratio of 20 (Figure 5A). The zeta potential of the siRNA/CRT nanoparticles increased with rising N/P ratios, with the surface charge reaching approximately +20 mV at a N/P ratio of 20 (Figure 5B). These findings suggest that increasing the N/P ratio improves the stability of the nanoparticles. Cytotoxicity assays demonstrated that peptide **CRT** had no significant cytotoxicity toward T cells at a concentration of 100 μM (N/P = 20), highlighting the biocompatibility of the system (Figure 5C).

https://doi.org/10.1021/acsnanomed.5c00151
ACS Nano Med. XXXX, XXX, XXX−XXX

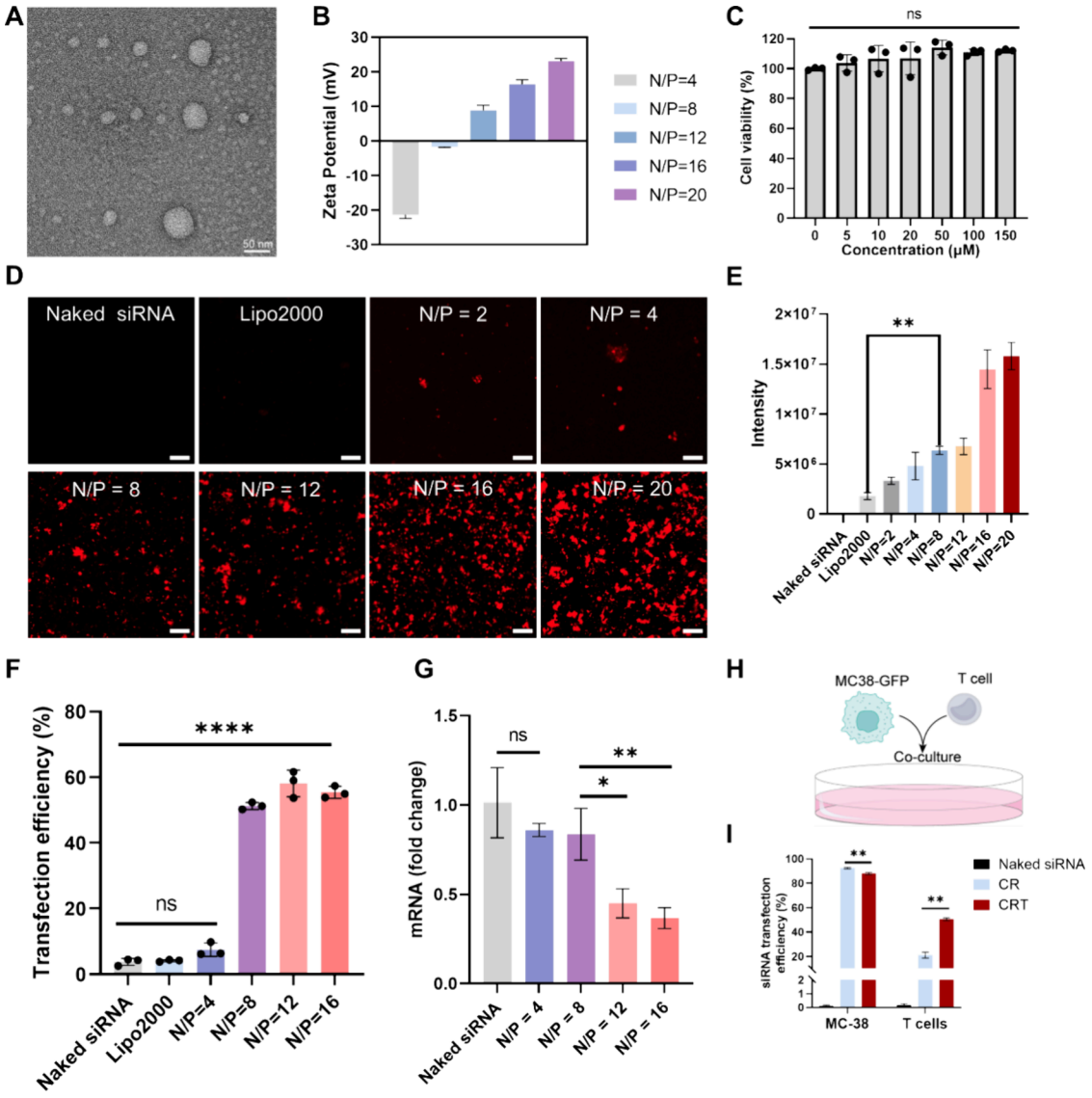

Figure 5. T cells-targeted siRNA delivery with peptide **CRT**. (A) TEM images of siRNA/CRT NPs at an N/P ratio of 20. (B) Zeta potential of siRNA/**CRT** NPs at various N/P ratios. (C) Cytotoxicity of peptide **CRT** against CTLL-2 after treatment for 24 h. (D) Representative CLSM images of $CD3^+$ T cells after treatment with siRNA/**CRT** NPs for 6 h. Scale bar is 50 μm. (E) Quantification of the MFI of $CD3^+$ T cells after transfection with siRNA-Cy5 using peptide **CRT**. (F) siRNA delivery efficiency of peptide **CRT** in T cells after treatment for 6 h. (G) Quantitative analysis of PD-1 knockdown efficiency in PD-1-CTLL-2 cells following 48 h transfection with siPD-1 using peptide **CRT** at different N/P ratios. (H) Coculture model of MC38-GFP cells and T cells. (I) siRNA transfection efficiency of **CRT** in the coculture model. Data are depicted as mean ± SD. Statistical analysis is calculated using one-way ANOVA analysis. *$p < 0.05$, **$p < 0.01$, ***$p < 0.001$, and ****$p < 0.0001$.

The CLSM images demonstrated that the **CRT** peptide enhanced siRNA delivery to T cells compared to that of the CR peptide (Figure 5D). The mean fluorescence intensity (MFI) of T cells in the CRT group was significantly higher than that in the Lipo2000 group (Figure 5E), confirming the superior transfection capability of **CRT**. The siRNA delivery efficiency of peptide **CRT** reached approximately 60% at an N/P ratio of 12 (Figure 5F). To assess the functional efficacy of the delivery system, we examined *PD-1* knockdown in PD-1-CTLL-2 cells following 48 h of transfection with PD-1 siRNA sequences using peptide **CRT** (Table S1).

We screened a series of PD-1 siRNA sequences to identify those with the most effective knockdown capability (Figure S16). Quantitative PCR (qPCR) analysis revealed that siPD-1 delivered by CRT nanoparticles efficiently silenced PD-1 expression in PD-1-CTLL-2 cells at an N/P ratio of 12 (Figure 5G), demonstrating the functional efficacy of the delivery system. Finally, we evaluated the T cell-targeting effect of **CRT** in a coculture model of MC38-GFP cells and T cells (Figure 5H). Compared to peptide CR, **CRT** improved siRNA delivery efficiency in CTLL-2 cells while decreasing siRNA delivery efficiency in MC38 cells (Figure 5I). These results highlight the selective targeting capability of **CRT** for T cells, making it a promising tool for targeted immunotherapy (Figure 5I).

siRNA Selectively Transduces Specific Immune Cells in the Tumor Microenvironment

To further evaluate the targeted delivery efficiency of siRNA using peptide **CRD**, we cocultured MC38-GFP cells and DC2.4 cells and treated them with siRNA/CRD NPs at an N/P ratio of 4 for 6 h (Figure 6A). The siRNA transfection efficiency mediated by **CRD** was approximately 55% in MC38 cells and 95% in DC2.4 cells, indicating a strong preference for

https://doi.org/10.1021/acsnanomed.5c00151
ACS Nano Med. XXXX, XXX, XXX−XXX

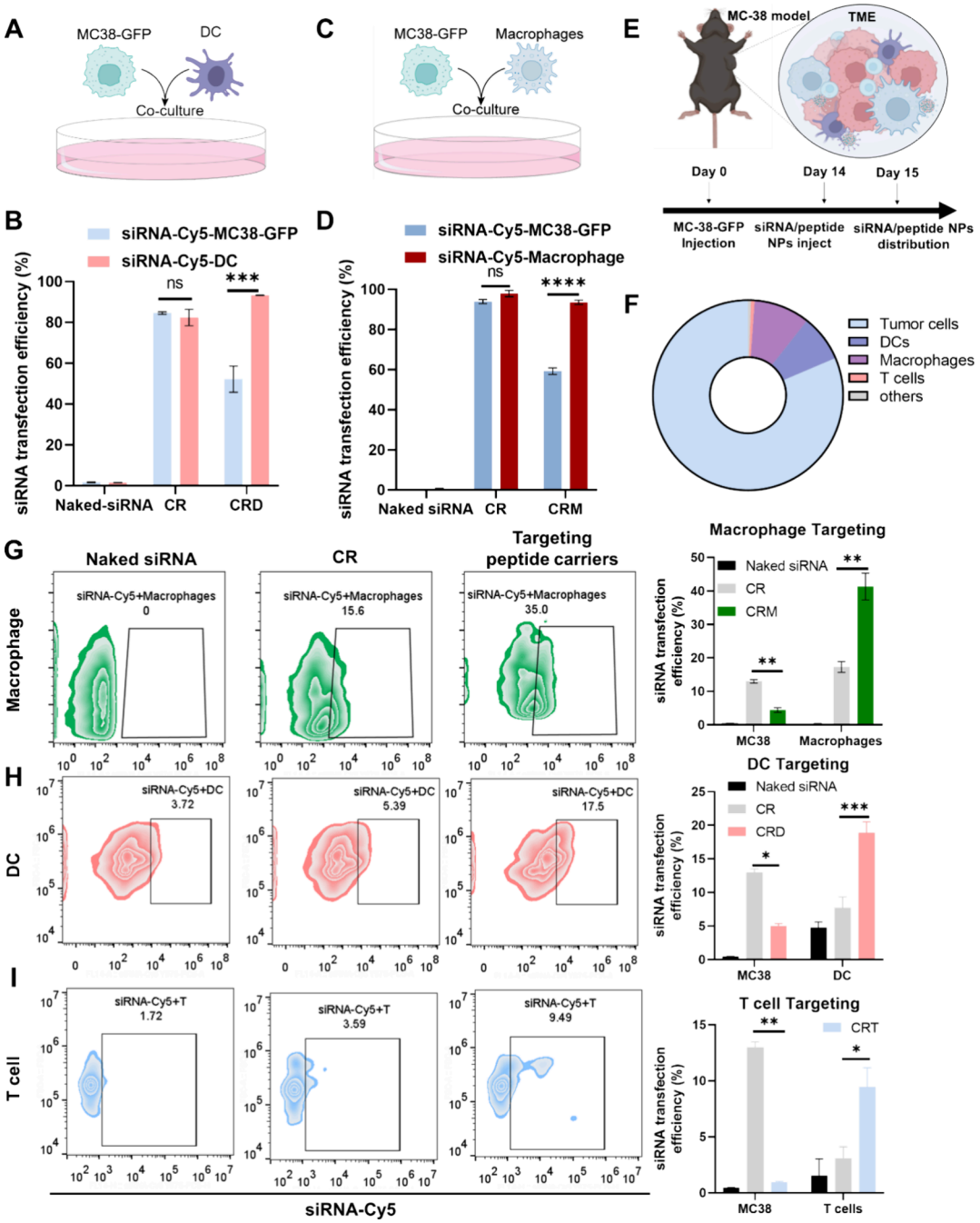

Figure 6. siRNA targeted delivery to specific immune cells with modular peptide carriers in complex environments. (A) **CRD**-mediated DCs targeted siRNA delivery in the coculture model (MC38-GFP: DC2.4 = 1:1). (B) siRNA delivery efficiency in DC2.4 and MC38 in the coculture model after transfection with **CRD** for 6 h. (C) **CRM** mediated macrophages targeted siRNA delivery in the coculture model (MC38-GFP: BMDM = 1:1). (D) siRNA delivery efficiency in BMDM and MC38 in the coculture model after transfection with CRM for 6 h. (E) siRNA targeted delivery to specific cells with modular peptides in the tumor microenvironment. (F) Cell type composition of the MC38 tumor microenvironment. (G) Macrophages targeted siRNA delivery with **CRM** in the MC38 tumor model. (H) DCs targeted siRNA delivery with **CRD** in the MC38 tumor model. (I) T cells targeted siRNA delivery with **CRT** in the MC38 tumor model. Data are depicted as mean ± SD. Statistical analysis is calculated using one-way ANOVA analysis. *p < 0.05, **p < 0.01, ***p < 0.001, and ****p < 0.0001.

dendritic cell transfection (Figure 6B). In comparison, peptide **CR** showed a lower delivery efficiency and less specificity, with **CRD** demonstrating both enhanced targeting and more efficient siRNA delivery to dendritic cells (Figure S17). Next, we established a coculture model of MC38-GFP cells and macrophages (Figure 6C). In this system, **CRM** achieved 60% transfection efficiency in MC38 cells and 95% in macrophages. **CRM** displayed selective targeting of macrophages, with an approximately 40% higher transfection efficiency in macrophages compared to MC38 cells. This further highlights the enhanced specificity of **CRM** for macrophages over tumor cells (Figure 6D, Figure S18). Furthermore, siRNA/peptide NPs designed for immune cell targeting demonstrated minimal cytotoxicity toward immune cell populations (Figure S19).

To investigate whether the modular peptide-based siRNA delivery systems can target immune cells in a more complex

https://doi.org/10.1021/acsnanomed.5c00151
ACS Nano Med. XXXX, XXX, XXX−XXX

environment, we established an MC38 tumor model by subcutaneously injecting MC38-GFP cells into 6−8-week-old C57BL/6J mice (Figure 6E). In the MC38 tumor microenvironment, MC38 cells make up about 80% of the cell population, macrophages approximately 10%, dendritic cells (DCs) 7−8%, and T cells around 0.5−1% (Figure 6F, Figure S20). We injected siRNA/CRM NPs into the MC38 tumor and analyzed their ability to deliver siRNA to macrophages in this complex environment. Flow cytometry analysis revealed that peptide **CRM** significantly improved macrophage siRNA delivery efficiency compared to peptide CR. Specifically, **CRM** achieved 41.31% siRNA delivery to macrophages, while peptide CR only delivered 17.25% (Figure 6G). This data underscore the superior macrophage-targeting capabilities of **CRM** within the TME.

Next, we evaluated the targeting efficiency of siRNA/CRD NPs in DCs within the TME. Peptide CRD achieved 18.89% and 6.17% siRNA delivery in DCs and MC38 cells, respectively, while more siRNA/CR assemblies were taken up by tumor cells than by DCs. This suggests that, despite the effective delivery to DCs, a significant fraction of siRNA was still preferentially internalized by tumor cells (Figure 6H). However, CRD did achieve more efficient DC-targeted siRNA delivery in vivo compared to peptide CR, indicating its potential for enhancing DC-targeted therapies in cancer.

Finally, we investigated whether the optimized T cell-targeting peptide (**CRT**) could improve T cell-specific siRNA delivery within the TME. After injecting siRNA/CRT NPs into the tumor, we observed that siRNA delivery efficiency was 0.94% in MC38 cells and 9.44% in T cells, highlighting a significant increase in T cell-targeted delivery compared to peptide **CR**, which showed much lower efficiency in T cells (Figure 6I). These findings suggest that **CRT** can significantly enhance T cell-specific siRNA delivery, offering a promising strategy for targeted immune modulation. Although the optimized modular peptide system significantly improves siRNA delivery to immune cells in the tumor microenvironment compared to the parent CR peptide, a degree of nonspecific uptake by tumor cells persists, likely due to passive accumulation. This modest selectivity highlights the need for further optimization. Future studies will focus on enhancing targeting specificity by fine-tuning ligand−receptor interactions, such as increasing ligand binding affinity, optimizing linker length to improve spatial orientation, and modulating nanoparticle surface charge to reduce nonspecific uptake.

CONCLUSION

Effective immune cell therapy requires a biocompatible targeted delivery system capable of selectively delivering genetic material to specific immune cells. In this study, we developed a modular peptide-based siRNA delivery system designed for targeted immune cell delivery. The system consists of three key components: a cell-penetrating peptide (CPP) to facilitate cellular uptake, an RNA-binding sequence $(RFH)_3$ to efficiently package negatively charged siRNA, and immune cell-targeting motifs for selective recognition of specific immune cell types. However, it should be noted that the modular peptide nanocarriers are more suitable for local treatment rather than systemic administration because of their limited stability in serum. Local administration can achieve a high local concentration of cargo-loaded nanocarriers, while minimizing systemic cytotoxicity. Given the central role of dysregulated immunity in fibrotic diseases, chronic inflammation, and the immune-suppressive environment, our system holds strong therapeutic potential for modulating the local immune system through siRNA delivery. For example, silencing immune checkpoints (PD-1, CTLA-4) in the tumor microenvironment can enhance antitumor immunity, while targeted knockdown of pro-inflammatory or pro-fibrotic mediators (IL-6, IL11) could alleviate tissue damage in inflammatory or fibrotic disorders.[46,47]

Our results demonstrate that **CRM** and **CRD** efficiently delivered siRNA to macrophages and dendritic cells, respectively, with effective endosomal escape. Notably, peptide **CRT** enhanced siRNA delivery to T cells, achieving the efficient silencing of *PD-1* in PD-1-CTLL-2 cells. Additionally, the modular nature of our delivery system allowed for selective targeting and siRNA delivery to distinct immune cell populations, both in coculture models and within the TME. This modular, peptide-based delivery platform represents a promising strategy for targeted gene delivery to immune cells and offers significant potential for the development of engineered immune cell therapies. The versatility of this system may facilitate the manufacturing of immune cells with tailored functionalities for therapeutic applications, including cancer immunotherapy and immune modulation.

METHODS

Materials

Fmoc-protected amino acids and 2-(1H-benzotriazole-1-yl)-1,1,3,3-tetramethyluronium hexafluorophosphate (HBTU) were purchased from GL Biochem (Shanghai, China). Rink-Amide resin (0.94 mmol/g) was obtained from Tianjin Nankai Hecheng Sci & Tech Co., Ltd. (Tianjin, China). N,N-Diisopropylethylamine (DIPEA), 2,2,2-trifluoroethanol (TFE), trifluoroacetic acid (TFA), and mannosamine were purchased from Aladdin. Recombinant murine GM-CSF and recombinant murine IL-4 cytokines were obtained from PeproTech (USA). The flow cytometry antibodies—anti-F4/80-BV421, anti-mouse CD11c-PE, and antimouse CD3-BV763—were purchased from BioLegend (USA). 3-(4,5-Dimethyl-2-thiazolyl)-2,5-diphenyl-2H-tetrazolium bromide (MTT) was purchased from Sangon Biotech (Shanghai, China). 1640 medium, FBS, and penicillin-streptomycin were purchased from Gibco. siRNA-Cy5 and mouse-derived *PD-1* siRNA sequences were synthesized by Sangon Biotech (Shanghai, China).

Cell Lines

DC2.4 cell line was purchased from CellCook and cultured with 1640 complete medium. RAW265.7 cell line was obtained from CellCook and cultured with 1640 complete medium. CTLL-2 is a clone of the cytotoxic T lymphocyte cell line, purchased from Procell and cultured in a 1640 complete medium supply with 100 U/mL recombinant IL-2 and 1.0 μg/mL Con A+1% P/S. The MC38-GFP cell was a gift from the laboratory of Dr. Jun Wei at the National Clinical Research Center for Blood Diseases. PD-1 overexpressing CTLL-2 cells were constructed by Hanbio Biotechnology Company, Ltd. (Shanghai, China).

Animals

C57BL/6J mice (6−8 weeks old) were purchased from Vital River Laboratory Animal Technology Co., Ltd. (Shanghai, China) and housed in specific pathogen free (SPF) conditions, with a 12 h light/dark cycle at a temperature of 25 °C. All animal experiments were performed following the protocols evaluated and approved by the Institutional Animal Care and Use Committee (IACUC) of Westlake University (IACUC Protocol #25-029-WHM).

Peptide Synthesis

The modular peptides were synthesized by standard solid-phase peptide synthesis (SPPS) according to our previous literature

https://doi.org/10.1021/acsnanomed.5c00151
ACS Nano Med. XXXX, XXX, XXX−XXX

report.[48] The mannose-modified peptide CRM was synthesized as follows. The side chain protected peptide was cleaved from 2-chlorotrityl chloride resin using a cleavage solution of TFE: DCM (2:8, v/v). Subsequently, 50 mg of the side chain-protected peptide was dissolved in 10 mL of DMF, and D-mannosamine hydrochloride (3 equiv) and HBTU (2 equiv) were added. The pH was adjusted to approximately 8 with DIPEA. The reaction mixture was stirred overnight, after which the solvent was removed by rotary evaporation. The peptide was then deprotected using a TFA/H_2O/TIS mixture (95:2.5:2.5, v/v/v). The crude product was precipitated with diethyl ether, purified by preparative HPLC, and characterized by analytical HPLC and MALDI-TOF mass spectrometry.

Formulation of Peptide and siRNA Complexes

A peptide stock solution with a concentration of 2 mM was prepared. To form peptide/siRNA nanoparticles, the diluted peptide was added to siRNA in RNase-free H_2O at various N/P ratios of 4, 8, 12, 16, and 20 (the ratio of nitrogen residues in the peptide to phosphate groups in the nucleic acid). The system was incubated for 45 min to allow for self-assembly into nanoparticles (NPs).

Harvest of BMDMs and BMDCs

BMDMs and BMDCs were isolated from 6 to 8-week-old C57BL/6J mice according to our previous protocol. BMDMs were cultured in complete 1640 medium supplemented with 20 ng/mL GM-CSF for 1 week. BMDCs were cultured in complete 1640 medium supplemented with 20 ng/mL of GM-CSF and 20 ng/mL of IL-4. Additionally, half of the medium was replaced every 3 days.

Harvest of $CD3^+$ T Cells from the Mouse Spleen

$CD3^+$ T cells were isolated from the spleens of 6−8-week-old C57BL/6J mice. The spleen was ground on a 70 μm cell strainer, and cells were collected with 5−10 mL of cold PBS buffer into a new tube. The cell suspension was centrifuged at 300g for 5 min at 4 °C, and the supernatant was carefully aspirated. Red blood cells were lysed using a Red Blood Cell Lysis Buffer. After lysis, the cells were resuspended in up to 4 mL of MojoSort Buffer, filtered through a 70 μm cell strainer, centrifuged again at 300g for 5 min, and resuspended in an appropriate volume of MojoSort Buffer. The cell concentration was determined, and cells were adjusted to a final concentration of 1×10^8 cells/mL.

Subsequently, 10 μL of Biotin-Antibody Cocktail was added, and the mixture was gently vortexed and incubated on ice for 15 min. Then, 10 μL of Nanobeads per 10^7 cells was added, mixed thoroughly, and incubated on ice for an additional 15 min. After incubation, 2.5 mL of MojoSort Buffer was added to the tube, which was then placed in a magnetic separator for 5 min. The unlabeled fraction was carefully poured off, and the retained labeled cells ($CD3^+$ T cells) were collected and cultured in complete 1640 medium containing 10 ng/mL of recombinant IL-2.

TEM of siRNA/Peptide Assemblies

The morphology of siRNA/peptide assemblies was characterized using a Talos L120C 120 kV transmission electron microscope (TEM, ThermoFisher, USA). First, a 5 μL sample was applied to a carbon-coated grid, and excess liquid was carefully blotted away by using filter paper. The sample was then stained with 5 μL of 2% uranyl acetate for 1 min. After removal of the excess stain and vacuum drying, the sample was directly examined using transmission electron microscopy (TEM).

Cryo-EM of siRNA/CRM NPs

Here, 3−4 μL of siRNA/CRM nanoparticles (NPs) was applied to the grid at 4 °C and 100% humidity. After a 30 s incubation, excess liquid was blotted with filter paper for 4 s (blotting time optimized per sample). The grid was then rapidly plunged into liquid ethane and cooled by liquid nitrogen using a Vitrobot Mark IV (Thermo Fisher Scientific) or a manual plunger. Vitrified grids were stored under liquid nitrogen until imaging. Imaging was performed on a 200 kV cryotransmission electron microscope (Thermo Fisher Scientific) equipped with a field emission gun and a direct electron detector.

DLS of siRNA/Peptide Complexes

The hydrodynamic diameters and zeta potential of siRNA/peptide complexes in H_2O (pH 7.4) were measured by dynamic light scattering (DLS) using a BI-200SM NanoBrook ZetaPALS at 25 °C. The siRNA/CRD complexes were prepared at N/P ratios of 1, 2, 3, and 4 using a constant 1 μg of siRNA for particle preparation. The siRNA/CRM nanoparticles (NPs) and siRNA/CRT complexes were prepared at N/P ratios of 4, 8, 12, 16, and 20. Each sample was analyzed for 90 s, and the measurement was repeated three times.

Cytotoxicity Test

To evaluate the cytotoxicity of the modular peptide, 2×10^4 cells/well were seeded in 96-well plates and cultured for 12 h. Subsequently, the peptide was added at different concentrations, and the cells were incubated for 24 h. Here, 10 μL of 5 mg/mL 3-(4,5-dimethylthiazol-2-yl)-2,5-diphenyltetrazolium bromide (MTT) was then added to each well and incubated for 4 h. After incubation, 100 μL of a SDS-HCl solution was added to each well and incubated overnight. Finally, the absorbance was measured at 490 nm using a microplate reader (Varioskan Lux, Thermo Fisher, USA).

siRNA Transfection with Modular Peptides

Immune cells were seeded in 24-well plates at a density of 1×10^5 cells/well and incubated overnight. The siRNA-Cy5/peptide complexes (1 μg siRNA/well) were added at various N/P ratios and incubated for 6 h. Subsequently, we analyzed the siRNA transfection efficiency by using flow cytometry and confocal laser scanning microscopy (CLSM).

Quantification of *PD-1* Silencing in PD-1-CTLL-2 Cells Using qPCR

PD-1-CTLL-2 cells were seeded in 24-well plates and cultured for 12 h. *PD-1* siRNA was transfected with peptide CRT at an N/P ratio of 12. After 48 h of treatment, PD-1-CTLL-2 cells were collected and washed with PBS. Total RNA was extracted using TRIzol (no. 15596018, Thermo Fisher) and quantified using a NanoDrop (Thermo Fisher). The mRNA was purified, and cDNA was synthesized using the NovoScript first Strand cDNA Synthesis SuperMix (gDNA Purge) Kit (E047−01B, Novoprotein). Real-time PCR was then performed in triplicate using a NovoStart SYBR qPCR SuperMix Plus Kit (E096−01B, Novoprotein) on a Bio-Rad CFX96 real-time PCR system. The relative expression of PD-1 was normalized to the expression level of β-actin. The primers for PD-1 are listed in the Supporting Information.

Immune Cell Distribution of siRNA in the MC38 Tumor Microenvironment

MC38-GFP cells (1×10^6 cells in 50 μL) were subcutaneously injected into 6−8-week-old C57BL/6J mice. After 2 weeks, siRNA-Cy5/CR complexes, siRNA-Cy5/CRM NPs, siRNA-Cy5/CRD NPs, and siRNA-Cy5/CRT NPs were injected into the tumors. After 12 h, tumor-bearing mice were euthanized, and the tumors were carefully dissected using sterile scissors and forceps, removing as much fat and necrotic tissue as possible. The tumor tissue was placed into a sterile centrifuge tube containing precooled PBS. The tumors were then cut into 1−3 mm^3 pieces using sterile scissors and incubated in 5 mL of digestion solution containing 1 mg/mL Collagenase IV and 20 μg/mL DNase I in HBSS at 37 °C for 1 h. After digestion, the suspension was filtered through a 70 μm cell strainer into a new centrifuge tube to remove undigested tissue and debris. Red blood cells were lysed by adding 5 mL of red blood cell lysis buffer for 5 min, and then the lysis was stopped by adding 10 mL of PBS. The suspension was centrifuged at 300g for 5 min, and the supernatant was discarded. The cells were stained with anti-F4/80-BV421, anti-CD11c-PE, and anti-CD3-BV763 antibodies and analyzed by flow cytometry.

■ ASSOCIATED CONTENT

Supporting Information

The Supporting Information is available free of charge at https://pubs.acs.org/doi/10.1021/acsnanomed.5c00151.

https://doi.org/10.1021/acsnanomed.5c00151
ACS Nano Med. XXXX, XXX, XXX−XXX

Peptide synthesis (HPLC and LC-MS spectrum), peptide/siRNA NPs characterizations, cell cytotoxicity, confocal images of cells, and flow cytometry (PDF)

AUTHOR INFORMATION

Corresponding Author

Huaimin Wang − *State Key Laboratory of Gene Expression, School of Science, Westlake University, Hangzhou 310030 Zhejiang Province, China; Department of Chemistry, School of Science, Westlake University, Hangzhou 310030 Zhejiang Province, China;* orcid.org/0000-0002-8796-0367; Email: wanghuaimin@westlake.edu.cn

Authors

Nan Kong − *State Key Laboratory of Gene Expression, School of Science, Westlake University, Hangzhou 310030 Zhejiang Province, China; Department of Chemistry, School of Science, Westlake University, Hangzhou 310030 Zhejiang Province, China*

Yueying Liu − *State Key Laboratory of Gene Expression, School of Science, Westlake University, Hangzhou 310030 Zhejiang Province, China; Department of Chemistry, School of Science, Westlake University, Hangzhou 310030 Zhejiang Province, China*

Liheng Lu − *State Key Laboratory of Gene Expression, School of Science, Westlake University, Hangzhou 310030 Zhejiang Province, China; Department of Chemistry, School of Science, Westlake University, Hangzhou 310030 Zhejiang Province, China*

Complete contact information is available at: https://pubs.acs.org/10.1021/acsnanomed.5c00151

Author Contributions

H.W. conceived this work. N.K. performed the experiments and collected data. N.K. and H.W. analyzed the data and wrote the manuscript with input from the other authors. Y.L. and L.L. help with the animal experiments. All authors read and approved the manuscript.

Funding

This work was supported by Zhejiang Provincial Natural Science Foundation of China (2025SDXT002) and the National Natural Science Foundation of China (U24A2076).

Notes

The authors declare the following competing financial interest(s): N. K. and H.M. are inventors on a pending patent related to this work filed by China.

ACKNOWLEDGMENTS

This work was supported by State Key Laboratory of Gene Expression. We thank the Instrumentation and Service Center for Molecular Sciences, Instrumentation and Service Center for Physical Sciences, and Biomedical Research Core Facilities at Westlake University for assistance with measurements.

REFERENCES

(1) Rurik, J. G.; Tombacz, I.; Yadegari, A.; Mendez Fernandez, P. O.; Shewale, S. V.; Li, L.; Kimura, T.; Soliman, O. Y.; Papp, T. E.; Tam, Y. K.; Mui, B. L.; Albelda, S. M.; Pure, E.; June, C. H.; Aghajanian, H.; Weissman, D.; Parhiz, H.; Epstein, J. A. CAR T cells produced in vivo to treat cardiac injury. *Science* **2022**, *375* (6576), 91−96.

(2) Liu, C.; Shi, Q. Q.; Huang, X. A.; Koo, S.; Kong, N.; Tao, W. mRNA-based cancer therapeutics. *Nat. Rev. Cancer* **2023**, *23* (8), 526−543.

(3) Gupta, A.; Rudra, A.; Reed, K.; Langer, R.; Anderson, D. G. Advanced technologies for the development of infectious disease vaccines. *Nat. Rev. Drug Discovery* **2024**, *23* (12), 914−938.

(4) Irvine, D. J.; Maus, M. V.; Mooney, D. J.; Wong, W. W. The future of engineered immune cell therapies. *Science* **2022**, *378* (6622), 853−858.

(5) Zhang, F.; Parayath, N. N.; Ene, C. I.; Stephan, S. B.; Koehne, A. L.; Coon, M. E.; Holland, E. C.; Stephan, M. T. Genetic programming of macrophages to perform anti-tumor functions using targeted mRNA nanocarriers. *Nat. Commun.* **2019**, *10*, 3974.

(6) Chen, C.; Jing, W. Q.; Chen, Y.; Wang, G. Y.; Abdalla, M.; Gao, L.; Han, M. S.; Shi, C. D.; Li, A. N.; Sun, P. Intracavity generation of glioma stem cell-specific CAR macrophages primes locoregional immunity for postoperative glioblastoma therapy. *Sci. Transl Med.* **2022**, *14* (656), eabn1128.

(7) Rao, L.; Zhao, S. K.; Wen, C. R.; Tian, R.; Lin, L. S.; Cai, B.; Sun, Y.; Kang, F.; Yang, Z.; He, L. C.; et al. Activating macrophage-mediated cancer immunotherapy by genetically edited nanoparticles. *Adv. Mater.* **2020**, *32* (47), No. e2004853.

(8) Singh, A.; Chakraborty, S.; Wong, S. W.; Hefner, N. A.; Stuart, A.; Qadir, A. S.; Mukhopadhyay, A.; Bachmaier, K.; Shin, J. W.; Rehman, J.; et al. Nanoparticle targeting of de novo profibrotic macrophages mitigates lung fibrosis. *P. Natl. Acad. Sci. USA* **2022**, *119* (15), No. e2121098119.

(9) Kastenmüller, W.; Kastenmüller, K.; Kurts, C.; Seder, R. A. Dendritic cell-targeted vaccines - hope or hype? *Nat. Rev. Immunol* **2014**, *14* (10), 705−711.

(10) Barbier, A. J.; Jiang, A. Y. J.; Zhang, P.; Wooster, R.; Anderson, D. G. The clinical progress of mRNA vaccines and immunotherapies. *Nat. Biotechnol.* **2022**, *40* (6), 840−854.

(11) Stadtmauer, E. A.; Fraietta, J. A.; Davis, M. M.; Cohen, A. D.; Weber, K. L.; Lancaster, E.; Mangan, P. A.; Kulikovskaya, I.; Gupta, M.; Chen, F.; et al. CRISPR-engineered T cells in patients with refractory cancer. *Science* **2020**, *367* (6481), No. eaba7365.

(12) Zhang, J. L.; Chen, C. R.; Fu, H.; Yu, J.; Sun, Y.; Huang, H.; Tang, Y. J.; Shen, N.; Duan, Y. R. MicroRNA-125a-Loaded Polymeric Nanoparticles Alleviate Systemic Lupus Erythematosus by Restoring Effector/Regulatory T Cells Balance. *ACS Nano* **2020**, *14* (4), 4414−4429.

(13) Maude, S. L.; Frey, N.; Shaw, P. A.; Aplenc, R.; Barrett, D. M.; Bunin, N. J.; Chew, A.; Gonzalez, V. E.; Zheng, Z. H.; Lacey, S. F.; et al. Chimeric antigen receptor T cells for sustained remissions in leukemia. *New Engl J. Med.* **2014**, *371* (16), 1507−1517.

(14) Berdecka, D.; De Smedt, S. C.; De Vos, W. H.; Braeckmans, K. Non-viral delivery of RNA for therapeutic T cell engineering. *Adv. Drug Deliver. Rev.* **2024**, *208*, 115215 DOI: ARTN 115215.

(15) Alsaiari, S. K.; Eshaghi, B.; Du, B. J.; Kanelli, M.; Li, G.; Wu, X. H.; Zhang, L. X.; Chaddah, M.; Lau, A.; Yang, X.; et al. CRISPR-Cas9 delivery strategies for the modulation of immune and non-immune cells. *Nat. Rev. Mater.* **2025**, *10* (1), 44−61.

(16) Porter, D. L.; Levine, B. L.; Kalos, M.; Bagg, A.; June, C. H. Chimeric antigen receptor-modified T cells in chronic lymphoid leukemia. *New Engl J. Med.* **2011**, *365* (8), 725−733.

(17) Russell, S.; Bennett, J.; Wellman, J. A; Chung, D. C; Yu, Z.-F.; Tillman, A.; Wittes, J.; Pappas, J.; Elci, O.; McCague, S.; Cross, D.; Marshall, K. A; Walshire, J.; Kehoe, T. L; Reichert, H.; Davis, M.; Raffini, L.; George, L. A; Hudson, F P.; Dingfield, L.; Zhu, X.; Haller, J. A; Sohn, E. H; Mahajan, V. B; Pfeifer, W.; Weckmann, M.; Johnson, C.; Gewaily, D.; Drack, A.; Stone, E.; Wachtel, K.; Simonelli, F.; Leroy, B. P; Wright, J F.; High, K. A; Maguire, A. M Efficacy and safety of voretigene neparvovec (AAV2-hRPE65v2) in patients with RPE65-mediated inherited retinal dystrophy: a randomised, controlled, open-label, phase 3 trial (vol 390, pg 849, 2017). *Lancet* **2017**, *390* (10097), 849.

(18) Kuzmin, D. A.; Shutova, M. V.; Johnston, N. R.; Smith, O. P.; Fedorin, V. V.; Kukushkin, Y. S.; van der Loo, J. C. M.; Johnstone, E.

C. The clinical landscape for AAV gene therapies. *Nat. Rev. Drug Discovery* **2021**, *20* (3), 173−174.
(19) Strebinger, D.; Frangieh, C. J.; Friedrich, M. J.; Faure, G.; Macrae, R. K.; Zhang, F. Cell type-specific delivery by modular envelope design. *Nat. Commun.* **2023**, *14* (1), 5141.
(20) Nyberg, W. A.; Ark, J.; To, A.; Clouden, S.; Reeder, G.; Muldoon, J. J.; Chung, J.-Y.; Xie, W. H.; Allain, V.; Steinhart, Z.; Chang, C.; Talbot, A.; Kim, S.; Rosales, A.; Havlik, L. P.; Pimentel, H.; Asokan, A.; Eyquem, J. An Evolved AAV Variant Enables Efficient Genetic Engineering of Murine T Cells. *Cell* **2023**, *186* (2), 446−460.
(21) Madigan, V.; Zhang, F.; Dahlman, J. E. Drug delivery systems for CRISPR-based genome editors. *Nat. Rev. Drug Discovery* **2023**, *22* (11), 875−894.
(22) Dilliard, S. A.; Siegwart, D. J. Passive, active and endogenous organ-targeted lipid and polymer nanoparticles for delivery of genetic drugs. *Nat. Rev. Mater.* **2023**, *8* (4), 282−300.
(23) Polack, F. P.; Thomas, S. J.; Kitchin, N.; Absalon, J.; Gurtman, A.; Lockhart, S.; Perez, J. L.; Perez Marc, G.; Moreira, E. D.; Zerbini, C.; Bailey, R.; Swanson, K. A.; Roychoudhury, S.; Koury, K.; Li, P.; Kalina, W. V.; Cooper, D.; Frenck, R. W.; Hammitt, L. L.; Tureci, O.; Nell, H.; Schaefer, A.; Unal, S.; Tresnan, D. B.; Mather, S.; Dormitzer, P. R.; Sahin, U.; Jansen, K. U.; Gruber, W. C. Safety and efficacy of the BNT162b2 mRNA Covid-19 vaccine. *New Engl J. Med.* **2020**, *383* (27), 2603−2615.
(24) Tretbar, U. S.; Rurik, J. G.; Rustad, E. H.; Sürün, D.; Köhl, U.; Olweus, J.; Buchholz, F.; Ivics, Z.; Fricke, S.; Blache, U. Non-viral vectors for chimeric antigen receptor immunotherapy. *Nat. Rev. Method Prime* **2024**, *4* (1), 74.
(25) Parayath, N. N.; Stephan, S. B.; Koehne, A. L.; Nelson, P. S.; Stephan, M. T. In vitro-transcribed antigen receptor mRNA nanocarriers for transient expression in circulating T cells in vivo. *Nat. Commun.* **2020**, *11* (1), 6080.
(26) Dammes, N.; Goldsmith, M.; Ramishetti, S.; Dearling, J. L. J.; Veiga, N.; Packard, A. B.; Peer, D. Conformation-sensitive targeting of lipid nanoparticles for RNA therapeutics. *Nat. Nanotechnol.* **2021**, *16* (9), 1030−1038.
(27) Nabih, N. W.; Hassan, H.; Preis, E.; Schaefer, J.; Babker, A.; Abbas, A. M.; Amin, M. U.; Bakowsky, U.; Fahmy, S. A. Antibody-functionalized lipid nanocarriers for RNA-based cancer gene therapy: advances and challenges in targeted delivery. *Nanoscale Adv.* **2025**, *7* (19), 5905−5931.
(28) Rosenblum, D.; Joshi, N.; Tao, W.; Karp, J. M.; Peer, D. Progress and challenges towards targeted delivery of cancer therapeutics. *Nat. Commun.* **2018**, *9*, 1410.
(29) Chen, M. Z.; Yuen, D.; McLeod, V. M.; Yong, K. W.; Smyth, C. H.; Herling, B. R.; Payne, T. J.; Fabb, S. A.; Belousoff, M. J.; Algarni, A.; et al. A versatile antibody capture system drives specific in vivo delivery of mRNA-loaded lipid nanoparticles. *Nat. Nanotechnol.* **2025**, *20* (9), 1273−1284.
(30) Attia, R. T.; Babker, A.; Nafie, M. S.; Saleh, F. A.; Abdelwareth, M. A.; Loutfy, E. M.; Alameen, A. A. M.; Fahmy, S. A. Mucoadhesive chitosan-coated boswellic acids nanoparticles as promising gastro-protective nanoagents via modulation of the RAS/ERK signaling pathway. *Discov Nano* **2025**, *20* (1), 190.
(31) Chen, C.; Jing, W.; Chen, Y.; Wang, G.; Abdalla, M.; Gao, L.; Han, M.; Shi, C.; Li, A.; Sun, P.; et al. Intracavity generation of glioma stem cell-specific CAR macrophages primes locoregional immunity for postoperative glioblastoma therapy. *Sci. Transl Med.* **2022**, *14* (656), No. eabn1128.
(32) Foss, D. V.; Muldoon, J. J.; Nguyen, D. N.; Carr, D.; Sahu, S. U.; Hunsinger, J. M.; Wyman, S. K.; Krishnappa, N.; Mendonsa, R.; Schanzer, E. V.; et al. Peptide-mediated delivery of CRISPR enzymes for the efficient editing of primary human lymphocytes. *Nat. Biomed Eng.* **2023**, *7* (5), 647−660.
(33) Eweje, F.; Ibrahim, V.; Shajii, A.; Walsh, M. L.; Ahmad, K.; Alrefai, A.; Miyasato, D.; Davis, J. R.; Ham, H.; Li, K. C.; et al. Self-assembling protein nanoparticles for cytosolic delivery of nucleic acids and proteins. *Nat. Biotechnol.* **2025**.
(34) Liu, H.; Song, Z.; Zhang, Y.; Wu, B.; Chen, D.; Zhou, Z.; Zhang, H.; Li, S.; Feng, X.; Huang, J.; Wang, H. De novo design of self-assembling peptides with antimicrobial activity guided by deep learning. *Nat. Mater.* **2025**, *24*, 1295−1306.
(35) Wu, B.; Liang, J.; Yang, X.; Fang, Y.; Kong, N.; Chen, D.; Wang, H. A programmable peptidic hydrogel adjuvant for personalized immunotherapy in resected stage tumors. *J. Am. Chem. Soc.* **2024**, *146* (12), 8585−8597.
(36) Tai, W. Y.; Gao, X. H. Functional peptides for siRNA delivery. *Adv. Drug Deliver Rev.* **2017**, *110*, 157−168.
(37) Chen, D.; Kong, N.; Wang, H. Leading-edge pulmonary gene therapy approached by barrier-permeable delivery system: a concise review on peptide system. *Adv. NanoBiomed. Res.* **2022**, *2* (12), 2200113.
(38) Chen, Y.; Chen, X.; Zhang, Y.; Wang, M.; Yang, M.; Wang, R.; Yan, X.; Shao, S.; Xin, H.; Hu, Q.; et al. Macrophage-specific in vivo RNA editing promotes phagocytosis and antitumor immunity in mice. *Sci. Transl Med.* **2025**, *17* (781), No. eadl5800.
(39) Puth, S.; Verma, V.; Hong, S. H.; Tan, W.; Lee, S. E.; Rhee, J. H. An all-in-one adjuvanted therapeutic cancer vaccine targeting dendritic cell cytosol induces long-lived tumor suppression through NLRC4 inflammasome activation. *Biomaterials* **2022**, *286*, 121542.
(40) Nyberg, W. A.; Ark, J.; To, A.; Clouden, S.; Reeder, G.; Muldoon, J. J.; Chung, J. Y.; Xie, W. H.; Allain, V.; Steinhart, Z.; et al. An evolved AAV variant enables efficient genetic engineering of murine T cells. *Cell* **2023**, *186* (2), 446−460.
(41) Moreno Herrero, J.; Stahl, T. B.; Erbar, S.; Maxeiner, K.; Schlegel, A.; Bacic, T.; Schumacher, J.; Cavalcanti, L. P.; Schroer, M. A.; Svergun, D. I.; Sahin, U.; Haas, H. Compact polyethylenimine-complexed mRNA vaccines. *Nat. Nanotechnol.* **2025**, *20* (9), 1323−1331.
(42) Kong, N.; Chen, D.; Wu, B.; Liang, J.; Zhou, Z.; Lu, H.; Li, Y.; Zhang, P.; Liu, H.; Wang, H. Structure-guided design of nucleosome-inspired nanoparticles for overcoming pulmonary barriers in fibrotic lung gene therapy. *Sci. Adv.* **2025**, *11* (46), No. eady0952.
(43) Guo, X. C.; Guo, M. Y.; Cai, R.; Hu, M. D.; Rao, L.; Su, W.; Liu, H.; Gao, F. E.; Zhang, X. Y.; Liu, J.; et al. mRNA compartmentalization via multimodule DNA nanostructure assembly augments the immunogenicity and efficacy of cancer mRNA vaccine. *Sci. Adv.* **2024**, *10* (47), No. eadp3680.
(44) Cirillo, S.; Tomeh, M. A.; Wilkinson, R. N.; Hill, C.; Brown, S.; Zhao, X. Designed Antitumor Peptide for Targeted siRNA Delivery into Cancer Spheroids. *ACS Appl. Mater. Interfaces* **2021**, *13* (42), 49713−49728.
(45) Hadianamrei, R.; Zhao, X. Current state of the art in peptide-based gene delivery. *J. Controlled Release* **2022**, *343*, 600−619.
(46) Chen, L. Co-inhibitory molecules of the B7-CD28 family in the control of T-cell immunity. *Nat. Rev. Immunol* **2004**, *4* (5), 336−347.
(47) Cui, L.; Chen, S. Y.; Lerbs, T.; Lee, J. W.; Domizi, P.; Gordon, S.; Kim, Y. H.; Nolan, G.; Betancur, P.; Wernig, G. Activation of JUN in fibroblasts promotes pro-fibrotic programme and modulates protective immunity. *Nat. Commun.* **2020**, *11* (1), 2795.
(48) Hu, L. B.; Li, Y.; Lin, X. H.; Huo, Y. C.; Zhang, H. Y.; Wang, H. M. Structure-based programming of supramolecular assemblies in living cells for selective cancer cell inhibition. *Angew. Chem. Int. Edit* **2021**, *60* (40), 21807−21816.

https://doi.org/10.1021/acsnanomed.5c00151
ACS Nano Med. XXXX, XXX, XXX−XXX